SANDIA REPORT
SAND99–8220
Unlimited Release
Printed February 1999

Condensation Pressures in Small Pores: An Analytical Model Based on Density Functional Theory

R. H. Nilson, S. K. Griffiths

Prepared by
Sandia National Laboratories
Albuquerque, New Mexico 87185 and Livermore, California 94550

Sandia is a multiprogram laboratory operated by Sandia Corporation, a Lockheed Martin Company, for the United States Department of Energy under Contract DE-AC04-94AL85000.

Sandia National Laboratories

Issued by Sandia National Laboratories, operated for the United States Department of Energy by Sandia Corporation.

Available to DOE and DOE contractors from
Office of Scientific and Technical Information
P.O. Box 62
Oak Ridge, TN 37831

Prices available from (615) 576-8401, FTS 626-8401

Available to the public from
National Technical Information Service
U.S. Department of Commerce
5285 Port Royal Rd
Springfield, VA 22161

NTIS price codes
Printed copy: A03
Microfiche copy: A01

SAND99-8220
Unlimited Release
Printed February 1999

Condensation Pressures in Small Pores: An Analytical Model Based on Density Functional Theory

Robert H. Nilson and Stewart K. Griffiths
Sandia National Laboratories
Livermore, California 94551-0969

Abstract

Integral methods are used to derive an analytical expression describing fluid condensation pressures in slit pores bounded by parallel plane walls. To obtain this result, the governing equations of Density Functional Theory (DFT) are integrated across the pore width assuming that fluid densities within adsorbed layers are spatially uniform. The thickness, density, and energy of these layers are expressed as composite functions constructed from asymptotic limits applicable to small and large pores. By equating the total energy of the adsorbed layers to that of a liquid-full pore, we arrive at a closed-form expression for the condensation pressure in terms of the pore size, surface tension, and Lennard-Jones parameters of the adsorbent and adsorbate molecules. The resulting equation reduces to the Kelvin equation in the large-pore limit. It further reproduces the condensation pressures computed by means of the full DFT equations for all pore sizes in which phase transitions are abrupt. Finally, in the limit of extremely small pores, for which phase transitions may be smooth and continuous, this simple analytical expression provides a good approximation to the apparent condensation pressure indicated by the steepest portion of the adsorption isotherm computed via DFT.

Introduction

Gas molecules in small pores condense to a liquid at pressures far below the bulk condensation pressure. This reduction in condensation pressure results from attractive forces between gas molecules and surrounding pore walls. Beginning at very low pressures, thin layers of closely packed molecules start to form on pore walls. With increasing pressure these adsorbed layers grow more dense and then thicker until reaching a point where the remaining gas in the pore condenses abruptly.

Adsorption and condensation are critical to many applications of porous materials including filtration, separation, and the storage of gases [1,2]. All of these processes depend on large specific surface areas to attract and store large quantities of gases in a relatively small physical volume. Process performance can often be enhanced by reducing pore sizes to near molecular dimensions. This generally maximizes specific surface area while also providing increased selectivity to gas species of differing molecular size. Moreover, in sufficiently small pores, attractive forces are doubled by the overlapping potential fields of opposing pore walls. The increased attraction further promotes adsorption and reduces condensation pressures, permitting low pressure storage of gases at near liquid densities.

Because adsorption and condensation depend strongly on pore size, these processes are often used to determine pore size distributions of microporous materials [3-7]. The amount of gas adsorbed by a material sample at a fixed temperature is first measured as a function of the external pressure. This adsorption isotherm is then compared with known measured or computed isotherms for various fixed pore sizes. For materials having very large pores, the measured isotherm should resemble the known isotherm of a flat surface, particularly at low pressures [8]. However, when smaller pores are present a large fraction of the total gas uptake will occur abruptly at the conden-

sation pressure corresponding to the most common pore size, as illustrated by the computed single-pore isotherms [7] displayed in Fig. 1. The measured gas uptake as a function of pressure thus provides a strong indication of pore size. This is true even for very small pores, in which the phase transition is continuous, since a small variation in pore size, say from 1.5 to 2.5 molecular diameters, shifts the phase transition pressure by two orders of magnitude. Further, when multiple pore sizes are present in a sample, the measured isotherm may be viewed as a weighted average of a basis set of single-pore isotherms.

In the past several years, detailed numerical models have been used by some researchers to compute single-pore isotherms and to deduce pore size distributions from measured isotherms [4-7]. Most of this computational work has been based on Density Functional Theory (DFT). In this approach, the time-mean density field within a pore is determined by solving integral equations relating the local chemical potential to the van der Waals attractions and hard sphere repulsions of surrounding material. DFT generally yields the same results as alternative Molecular Dynamic simulations and Monte Carlo methods, but requires much less computer time. Even so, computer times for DFT are usually measured in hours or days, and a considerable effort is required to develop a DFT computer code. Thus, there remains a need for a simple but reliable means for predicting adsorption and condensation based on analytical relationships involving only readily available material properties.

Here, we derive an analytical expression relating the condensation pressure to the pore width, surface tension, and Lennard-Jones parameters of the adsorbate and adsorbent molecules. This equation is obtained by employing approximate fluid density profiles in the governing equations of DFT. From these equations, the condensation pressure is determined by equating integral expressions for the total fluid energy before and after condensation. The total energy prior to condensation depends on the thickness, density and energy of adsorbed layers. These quantities are approximated by analytical expressions that correctly describe the asymptotic behavior in the limits of very small and very large pores and additionally provide a smooth transition between these limits.

The present condensation equation is in good agreement with detailed DFT calculations over the full range of pore sizes. It reduces to the Kelvin equation [1,2] in the limit of very large pores. At intermediate pore sizes our formulation resembles previous Modified Kelvin (MK) equations [4,9], but contains additional terms. Finally, in the small pore limit, our equation reduces to a form that is similar to those proposed by Horvath and Kawazoe [10] and Saito and Foley [11] in that the condensation pressure is related to the average intermolecular potential within the pore.

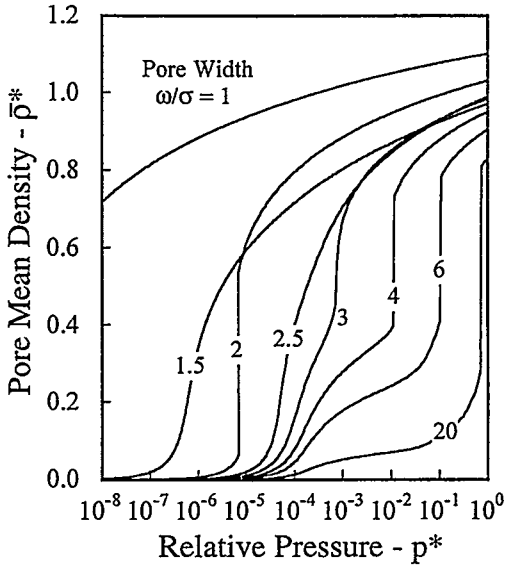

Figure 1. Adsorption isotherms computed by means of DFT for slit pores of width w. The phase transition from gas to liquid may be continuous in very small pores, but is always abrupt when pores are large.

In contrast to this earlier analytical work, the present equation provides very good estimates of the condensation pressure over the full range of pore sizes. Also, the present equation is derived from the rigorous and general theory of DFT. This provides a fundamental basis for understanding the result and for testing and improving the approximations made in deriving this simple but remarkably accurate expression.

Governing Equations of DFT

The fluid density distribution in a region of uniform temperature, T, and chemical potential, μ_∞, may be determined by minimizing the grand potential energy functional, Ω [4,5,12-14].

$$\Omega[\rho(\mathrm{r})] = \int \Big(f[\rho(\mathrm{r})] + \rho(\mathrm{r})[V(\mathrm{r}) - \mu_\infty] \Big) d\mathrm{r} \quad (1)$$

Here, V is the external potential induced by surrounding solid material, and f is the Helmholtz free energy consisting of an ideal gas component, a mean field attraction, U, and an excess hard sphere repulsion, $\Delta\psi$.

$$f = \rho(\mathrm{r}) \Big[kT \big(\ln [\Lambda^3 \rho(\mathrm{r})] - 1 \big) + \frac{1}{2} U(\mathrm{r}) + \Delta\psi(\mathrm{r}) \Big] \quad (2)$$

The logarithmic ideal gas component depends on the temperature and the local density, ρ, measured in molecular masses per unit volume, as well as the Boltzmann constant, k, and the deBroglie wave length, Λ.

The fluid attraction, U, is defined by a density weighted integral of a molecular pair potential function, u, over the surrounding fluid.

$$U(\mathbf{r}) = \int \rho(\mathbf{r}')\, u(|\mathbf{r}-\mathbf{r}'|)\, d\mathbf{r}' \qquad (3)$$

Here we employ a Lennard-Jones 6-12 potential at ranges between its cross over point, $r = \sigma$, and an arbitrary cutoff range, $r = r_{\max}$.

$$u(r) = 4\,\epsilon_{ff}\left[\left(\frac{\sigma}{r}\right)^{12} - \left(\frac{\sigma}{r}\right)^{6}\right], \quad \sigma < r < r_{\max} \qquad (4)$$

The potential vanishes, $u = 0$, outside this interval since it is presumed negligible at longer ranges, while the shorter range repulsions are described by a separate hard-sphere model. The molecular diameter, σ, and depth of the potential well, ϵ_{ff}, appearing in Eq. (4) are known approximately for common gases.

The excess fluid repulsion, $\Delta\psi$, is described by Tarazona's smoothed density model [5-7,13,14] derived from the Carnahan-Starling equation of state.

$$\Delta\psi(\widehat{\rho}) = kT\,\eta\,\frac{(4-3\eta)}{(1-\eta)^2} \quad \text{where} \quad \eta = \widehat{\rho}\,\frac{\pi d^3}{6} \qquad (5)$$

The normalized density, η, represents the volume fraction occupied by molecules having a hard sphere diameter, $d \approx \sigma$, and a smoothed density, $\widehat{\rho}$, obtained by averaging of the surrounding density field

$$\widehat{\rho}(\mathbf{r}) = \int \rho(\mathbf{r}')\,\omega(|\mathbf{r}-\mathbf{r}'|)\, d\mathbf{r}' \qquad (6)$$

using a linear weighting of densities within a sphere of radius σ.

$$\omega(r) = \frac{3}{\pi\sigma^3}\left(1-\frac{r}{\sigma}\right) \qquad (7)$$

This formulation of DFT provides good overall agreement with macroscopic data and with Monte Carlo simulations, including the formation and magnitude of sharp density peaks.

The external potential, V, is obtained by integrating the complete Lennard-Jones potential over the solid walls bounding the fluid. The solid density is usually assumed uniform over planar sheets of atoms spaced Δ apart, as in Steele's widely used formula [9].

$$v(z) = \epsilon_w\left[\frac{2}{5}\left(\frac{\sigma_{sf}}{z}\right)^{10} - \left(\frac{\sigma_{sf}}{z}\right)^{4} - \frac{\sigma_{sf}^4}{3\Delta(z+0.61\Delta)^3}\right] \qquad (8)$$

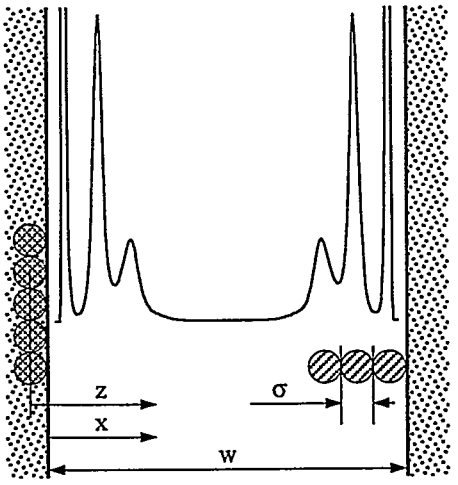

Figure 2. Schematic of adsorption on the walls of a slit pore. Density peaks of the first layers result from localization of molecular centers in the potential well of adjacent solid material. Successive layers are progressively less ordered and have less prominent peaks. Layer spacing is about one molecular diameter.

Here, z is the distance from the center plane of the surface layer of the solid atoms, σ_{sf} is the effective fluid-solid intermolecular diameter, and ϵ_w contains both the Lennard-Jones well depth, ϵ_{sf}, and the solid density, ρ_s.

$$\epsilon_w = 2\pi\rho_s\epsilon_{sf}\sigma_{sf}^2\Delta \qquad (9)$$

In a narrow slit bounded by two walls the external potential is then

$$V(x) = v\left(x+\frac{\sigma_{sf}}{2}\right) + v\left(w-x+\frac{\sigma_{sf}}{2}\right) \qquad (10)$$

where the position, x, and the pore width, w, are both measured from the surface of the first layer of atoms in the solid. This is as shown in Fig. 2.

Minimization of the potential energy functional, Ω, can now be accomplished by inserting the above definitions into Eq. (1), taking its variation with respect to $\rho(\mathbf{r})$, and equating the result to zero. The resulting Euler-Lagrange equation may be written as

$$kT\ln(\Lambda^3\rho) + U + \Delta\psi(\widehat{\rho}) + \widehat{\Delta\psi'} + V = \mu_\infty \qquad (11)$$

where

$$\widehat{\Delta\psi'}(\mathbf{r}) = \int \rho(\mathbf{r}')\,\omega(|\mathbf{r}-\mathbf{r}'|)\,\Delta\psi'(\widehat{\rho}(\mathbf{r}'))\, d\mathbf{r}' \qquad (12)$$

and

$$\Delta\psi'(\widehat{\rho}) = \frac{d}{d\widehat{\rho}}\left[\Delta\psi(\widehat{\rho})\right] = kT\,\frac{\pi d^3}{6}\,\eta\,\frac{(4-2\eta)}{(1-\eta)^3} \qquad (13)$$

For a chosen value of the ambient chemical potential and a specified external potential, V, the desired density distribution $\rho(\mathrm{r})$ may be determined by solving Eq. (11), usually by numerical means.

In numerical DFT, the region of interest is first subdivided into discrete cells wherein the density profile is either presumed to be uniform [4-6,13,14] or presumed to vary as an analytic function of position [7]. The integrals appearing in the Euler-Lagrange equation are then replaced by summations to obtain a system of coupled nonlinear equations that are solved for the mean cell densities. Here, we will use these numerical solutions [7] both to guide and to verify our derivation of an analytical expression for the condensation pressure. All such calculations will address nitrogen adsorption on graphite at 77 K with σ, Δ, σ_s, ρ_s, ϵ_{ff}, and ϵ_{sf} taken as 3.57 Å, 3.35 Å, 3.48 Å, 0.11 Å^{-3}, 1.86×10^{-14} erg/molecule and 0.78×10^{-14} erg/molecule. Before reviewing those results, however, it is useful to explore the application of DFT to fluids of uniform density.

Bulk Fluids

In regions where the fluid density is uniform, or nearly so, the integrals defining U and $\Delta\psi'$ in Eq. (11) can be evaluated explicitly to yield

$$kT\ln(\Lambda^3\rho)+\Delta\psi(\rho)+\rho(\Delta\psi'+\epsilon_{ff}C_{\mathrm{LJ}})+V=\mu_\infty \quad (14)$$

in which $C_{\mathrm{LJ}} \approx -11\sigma^3$ is the integral of u/ϵ_{ff} over an infinite domain. For a given value of the chemical potential, this equation generally has three roots, analogous to the multiple roots of a van der Waals equation of state. The smallest root is a gas density that differs very little from that given by the ideal gas law. Thus for simplicity, it is customary to describe the ambient gas properties using the familiar equations

$$\rho=\frac{p}{kT} \qquad \text{and} \qquad \mu_\infty = kT\ln(\Lambda^3\rho_\infty) \qquad (15)$$

in which the subscript ∞ indicates conditions far from adsorptive surfaces.

The largest root of Eq. (14) describes the density of a stable liquid. Its nominal or reference value, ρ_0, is evaluated in the absence of an external potential field at the bulk condensation pressure, p_0 where the bulk gas and liquid phases have equal energy. The liquid density, ρ, at any other pressure, p, in the presence of an external potential V must then satisfy

$$kT\ln(\frac{\rho}{\rho_0})+\Delta\psi(\rho)-\Delta\psi(\rho_0)+\rho(\Delta\psi'(\rho)+\epsilon_{ff}C_{\mathrm{LJ}})$$
$$-\rho_0(\Delta\psi'(\rho_0)+\epsilon_{ff}C_{\mathrm{LJ}})=-[V-kT\ln\left(\frac{p}{p_0}\right)] \quad (16)$$

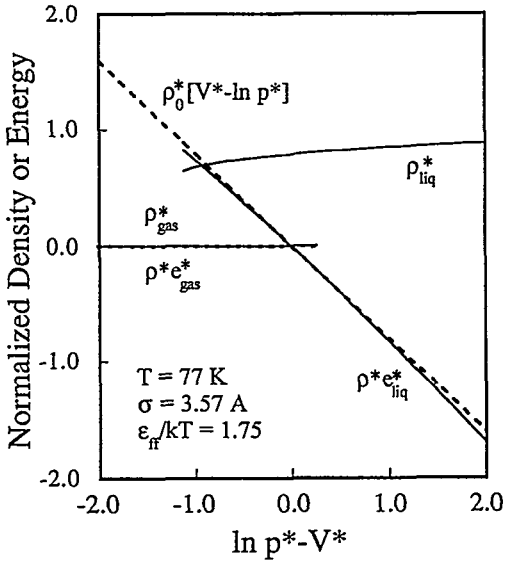

Figure 3. Bulk density and volumetric energy content of gas and liquid nitrogen. Liquid energy is well approximated by the linear approximation shown as a dotted line. Gas energy and density are negligible.

Thus, the deviation of the liquid density from its nominal value depends only on the difference between V and $kT\ln(p/p_0)$.

Similarly, the fluid energy per unit mass, relative to the same reference state, may be written as follows based on the definitions given in Eqs. (1) and (2).

$$e=kT\ln(\frac{\rho}{\rho_0})+\Delta\psi(\rho)-\Delta\psi(\rho_0)$$
$$+\frac{1}{2}\epsilon_{ff}C_{\mathrm{LJ}}(\rho-\rho_0)+[V-kT\ln\left(\frac{p}{p_0}\right)] \quad (17)$$

Since the liquid density rarely differs substantially from its nominal value, ρ_0, the liquid energy may be well approximated by the following expression.

$$e=V-kT\ln\left(\frac{p}{p_0}\right) \qquad (18)$$

As seen in Fig. 3, this approximation is more than adequate for present purposes, though it could be improved easily by constructing a Taylor expansion of the neglected terms about the reference state.

Figure 3 illustrates the calculated variation of the normalized density and volumetric energy content of liquid and gas nitrogen with pressure and external potential. The normalized variables used in the plot are defined as follows.

$$p^*=\frac{p}{p_0}, \quad \rho^*=\rho\sigma^3, \quad e^*=\frac{e}{kT}, \quad V^*=\frac{V}{kT} \quad (19)$$

From Eqs. (16) and (17) it is clear that both ρ^* and e^* depend only on the difference between V^* and $\ln p^*$. In keeping with expectations, Fig. 3 indicates that the gas density and energy are much smaller than those of the liquid and that the liquid density is relatively constant. Most importantly, the approximate expression for the liquid energy, given by Eq. (18) and shown by a dotted line in Fig. 3, differs only slightly from the exact calculation indicated by a solid line. Thus, we are well justified in using this approximation in subsequent equations.

Bulk liquid and gas solutions exist only within limited ranges of pressure and external potential. The gas is, of course, favored by low pressure and by the absence of an attractive (i.e., negative) external potential field. Bulk liquids are favored by high pressures and strongly attractive fields. As shown in Fig. 3, both solutions exist within a relatively narrow central range where V^* and $\ln p^*$ are of comparable magnitude. Bulk condensation occurs when V^* and $\ln p^*$ are nearly equal because the liquid energy is then very small and therefore comparable to that of the gas.

When the external potential field is either absent or spatially uniform, phase transitions will occur simultaneously at all locations. However, in the vicinity of solid surfaces or within small pores, variations in the potential field will cause liquid formation on solid surfaces at pressures much lower than those required for bulk condensation. These layers grow with increasing pressure until reaching the condensation pressure at which the fluid in the pore center abruptly condenses.

Density Profiles in Small Pores

The density variation across a narrow slit is illustrated in Fig. 4 for a pressure slightly less than the bulk condensation pressure, p_0. These profiles were calculated by numerically solving Eq. (11) on a grid having a spacing much smaller than molecular dimensions [7]. The density is assumed uniform in directions parallel to the pore walls, as appropriate when the pore width is small compared to its depth and lateral extent. The normalized variables appearing in the plot are all scaled by the molecular diameter.

$$x^* = \frac{x}{\sigma}, \quad w^* = \frac{w}{\sigma}, \quad \rho^* = \rho\sigma^3, \quad \widehat{\rho}^* = \widehat{\rho}\sigma^3 \qquad (20)$$

Also, since the density profiles are symmetric about the pore center, only the left half of the field is plotted.

Two solutions are shown in Fig. 4, each representing a local minimum of Ω. Although nearly identical near the pore wall, they approach substantially different values in the pore center. In that region, one solution has a low density typical of a gas while the other approaches a liquid density. Of these two solutions, the one applicable at any given pressure is that having the smaller value of the total energy Ω, obtained by cross-pore integration of the one dimensional profiles.

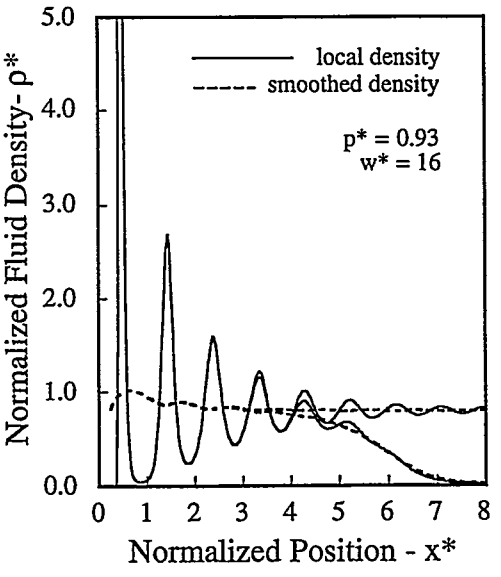

Figure 4. Density profile in the left half of a slit pore. Liquid and gas-like solutions are indicated by solid lines. Corresponding smoothed densities, shown dotted, are averaged over one molecular diameter.

$$\Omega = \int_0^w \rho e \, dx \qquad (21)$$

At pressures less than the condensation pressure, the gas-like solution has the lesser Ω, while at higher pressures the liquid-like solution becomes applicable. Thus, the condensation phase transition occurs when the two solutions have equal energy.

Strong oscillations of the local density are clearly apparent in the solid curves of Fig. 4. The prominent peak adjacent to the pore wall is coincident with the minimum point of the wall potential, V. As such, it is situated a distance roughly σ_{sf} from the center plane of the nearest atoms of the solid. Successive density peaks are separated by about one molecular diameter. With increasing distance from the wall, the width of the peaks increases and their amplitude decreases.

Figure 4 further shows that there is an excluded region immediately adjacent to the pore wall where the repulsion of wall molecules prevents the intrusion of adsorbate molecules. The outer edge of this exclusion zone is nearly coincident with the point where the

wall potential V passes through zero. Based on this criterion, the exclusion zone width, ϵ, is found to be nearly independent of the pore width, having a value of $\epsilon = 0.3238\sigma$ for the Steele potential of Eq. (8) and the carbon parameters given earlier.

The smoothed or locally averaged density, $\widehat{\rho}$, defined by Eq. (6) is also displayed in Fig. 4 by dashed curves. In contrast to the extreme variations in the local density, the smoothed density of the liquid-like solution is relatively uniform, falling from about unity at the pore walls to a value of $\widehat{\rho}^* \approx \rho_0^* \approx 0.8$ at the pore center. Similarly, the smoothed density of the gas-like solution remains nearly uniform over the adsorbed layers adjacent to the surface, but then falls to a much smaller gas density in the pore center. With increasing pressure, the thickness of the adsorbed layer increases, but the mean layer density and structure of the leading edge remain essentially the same.

Pore Condensation Equations

A closed-form expression for the condensation pressure is now derived by integrating the governing DFT equations across the pore, using approximate analytical profiles to describe the fluid density distribution. As seen on the right side of Fig. 5, the presumed density profile of the liquid-like solution is simply uniform at a value ρ_ℓ, which without much error may be taken as ρ_0. Similarly, the step-like density profile of gas-like solution is presumed to have a uniform value of ρ_g within the adsorbed layers, while the center density is assumed negligible. In keeping with numerical DFT calculations, the adsorbed layer density, ρ_g, must approach ρ_0 in large pores, but may be much smaller in narrow pores. The thickness of the adsorbed layers, denoted δ, is measured from the pore wall to the middle of the gas/liquid transition zone.

Since condensation occurs when gas and liquid solutions have equal energy, it is useful to express the total pore energy Ω in terms of the parameters that characterize the density profiles: ρ_0, ρ_g, and δ. Based on the definition of Ω in Eq. (21) and the approximation for e in Eq. (18), it follows that

$$\Omega = \int_0^w \rho\Big[V - kT\ln\Big(\frac{p}{p_0}\Big)\Big]dx \qquad (22)$$

Then, since the fluid density is assumed uniform in regions occupied by liquid and adsorbed layers, but is negligible elsewhere,

$$\Omega_\ell = \rho_\ell\Big[V_w - \widehat{w}\,kT\ln\Big(\frac{p}{p_0}\Big)\Big] \qquad (23)$$

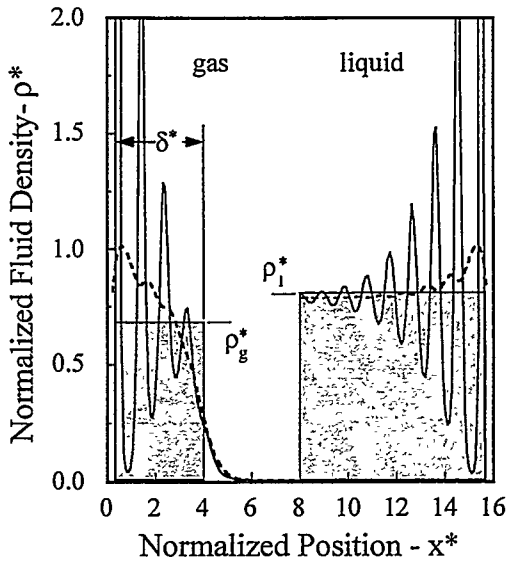

Figure 5. Schematic showing fluid density profiles just before condensation (left side of pore) and just after condensation (right side of pore). Approximate profiles, indicated by shading, represent average densities in regions occupied by liquid or adsorbed layers.

and

$$\Omega_g = \rho_g\Big[V_\delta - 2\widehat{\delta}\,kT\ln\Big(\frac{p}{p_0}\Big)\Big] + 2\Gamma \qquad (24)$$

in which the subscripts ℓ and g refer to the liquid-full and partially gas-filled pores of Fig. 5. The symbols $\widehat{w}$ and $\widehat{\delta}$ indicate respectively the portions of the pore width and the adsorbed layer that are occupied by high density fluid

$$\widehat{w} = w - 2\epsilon \qquad \text{and} \qquad \widehat{\delta} = \delta - \epsilon \qquad (25)$$

while V_w and V_δ denote integrals of the wall potential over these same regions.

$$V_w = 2\int_\epsilon^{w/2} V\,dx \quad \text{and} \quad V_\delta = 2\int_\epsilon^{\delta} V\,dx \qquad (26)$$

These integrals can be evaluated in closed form for any of the commonly used potentials (see Appendix).

The surface tension term, Γ, appearing in Ω_g accounts for the reduction in liquid energy at the interfaces between the adsorbed layers and the gas in the pore center. When the adsorbed layers are thick and have nominal liquid density, Γ is simply the nominal surface tension, γ. However, the associated deficit of attractive energy is roughly proportional to the density, ρ_g, of the adsorbed fluid and further, this deficit

must shrink to zero when the adsorbed layers merge in the pore center. We therefore make the following approximation

$$\Gamma = \gamma \frac{\rho_g}{\rho_0}\left(\frac{w-2\delta}{w}\right)\left(\frac{\delta-\epsilon}{\delta}\right) \tag{27}$$

The last term above recognizes that the surface energy resides mainly within the molecular layer nearest to the liquid/vapor interface and that this layer shrinks to zero as $\delta - \epsilon$ becomes small. No account is taken of similar energy deficits occurring at the liquid/solid contact, since these appear in both Ω_ℓ and Ω_g and are offsetting under conditions where surface tension is important.

By equating the energies of the liquid and gas solutions, Ω_ℓ and Ω_g, we arrive at the following equation relating the condensation pressure to the pore width, surface tension, fluid densities, and integrated wall potential.

$$\ln\left(\frac{p}{p_0}\right) = \frac{\rho_\ell V_w - \rho_g V_\delta - 2\Gamma}{kT(\rho_\ell \widehat{w} - 2\rho_g \widehat{\delta})} \tag{28}$$

This is the fundamental pore condensation equation (hereafter, NG equation). It is central to all that follows. To make it useful, however, we must first derive auxiliary relationships describing the thickness, $\widehat{\delta}$, and density, ρ_g, of the adsorbed layer in terms of the pressure and pore width.

In wide pores, the adsorbed layer remains thin compared to the pore width for pressure less than the condensation pressure. Thus, the external potential, V, within the adsorbed fluid is due almost entirely to the field of the adjacent pore wall. Under these conditions, the adsorbed layer thickness, $\widehat{\delta}$, can be approximated by

$$\widehat{\delta}_\infty^3 = -\frac{A}{\ln(p/p_0)} \quad \text{where} \quad A = \frac{\epsilon_w \sigma_{sf}^4}{3\Delta kT} \tag{29}$$

This relationship places the leading edge of the adsorbed fluid at roughly the point where $V = kT\ln(p/p_0)$, under a simplification of V that retains only the slowest decaying term in Eq. (8). This seems intuitively correct, since Eq. (18) indicates that the liquid energy vanishes at this point. Liquid situated further from the pore wall would have greater energy than the alternative zero-energy gas phase and thus could not exist. A more rigorous justification is provided by Sullivan [12] who derives Eq. (29) by minimizing Ω for an adsorbed liquid layer having a uniform density. His formula includes an additional term that accounts for changes in the self attractive energy of fluid in the central part of the adsorbed layer, an effect that is suppressed by applying a cutoff to the Lennard-Jones attraction of Eq. (4). Thus, for later comparison with numerical DFT results that apply a cutoff at 3σ, we will exclude this secondary term. If retained, this term would reduce the magnitude of A in Eq. (29) by an amount $2\pi\epsilon_{ff}/3\rho_0$, leading to a 20% reduction in calculated values of δ.

In narrow pores, the adsorbed layer thickness is equal to half the pore width.

$$\widehat{\delta}_0^3 = \left(\frac{\widehat{w}}{2}\right)^3 \tag{30}$$

This limit clearly applies to all pores having a width of two molecular diameters or less. In pores that small, each of the adsorbed layers is barely wide enough to accommodate a single molecule, so there is no opportunity for the layers to increase in thickness with increasing pressure. Instead, the layer density, ρ_g, increases with increasing pressure until reaching the point of condensation.

A smooth transition between the small and large pore asymptotes is constructed by forming the ratio of their product and their sum.

$$\widehat{\delta} = \left[\frac{\widehat{\delta}_\infty^3\,\widehat{\delta}_0^3}{\widehat{\delta}_\infty^3 + \widehat{\delta}_0^3}\right]^{1/3} \tag{31}$$

This composite always yields a value of $\widehat{\delta}$ that is smaller than either of the asymptotic values. The cubic form of the composite is inspired by the form of the upper asymptote and produces a sharper transition than a linear interpolation between the asymptotes, in keeping with numerical DFT results presented later.

The fluid density, ρ_g, within the adsorbed layers also appears in the condensation formula, Eq. (28), and must therefore be specified. Again, it is useful to examine the limits of large and small pores. As seen earlier in Fig. 4, the fluid density in a thick layer of adsorbed fluid is essentially equal to the nominal liquid density, ρ_0. However, Fig. 1 shows that the mean density, ρ_g, of the adsorbed layers in a pore of normalized width $w^* = 2$ is less than 0.1 just prior to condensation. Moreover, in still smaller pores the transition from gas to liquid occurs not as as a true discontinuity, but instead appears as a smooth and continuous transition. This is also apparent in Fig. 1. In this regime, the mean density at the onset of the continuous transition is essentially zero. A smooth transition between this limit of $\rho_g \to 0$ for narrow layers, and a density of $\rho_g \to \rho_0$ in thick layers is provided by the approximation

$$\rho_g = \rho_0\left(\frac{2\widehat{\delta}-1}{2\widehat{\delta}}\right) \tag{32}$$

with the understanding that $\rho_g = 0$ for layers thinner than $\widehat{\delta} = 1/2$. This cutoff is encountered when the corresponding pore width, $\widehat{w} = 2\widehat{\delta} = 1$, is clearly too small to accommodate a pair of layers. In slightly larger pores, a pair of layers may exist with the centers of adsorbed molecules on opposing walls staggered in a manner that reduces repulsions. The form of Eq. (32) is chosen mainly for simplicity and for consistency with detailed DFT simulations.

In closing this derivation, we emphasize that details of the approximate transition formulas for $\widehat{\delta}$ and ρ_g are not critical. It is necessary only that they preserve the correct asymptotic behavior in the limits of small and large pores.

Asymptotic Behavior of NG Equation

To better understand the fundamental nature of the NG equation, it is useful to examine its behavior in the limits of very small and very large pores. The small pore, or low pressure, asymptote of the analytical model is readily obtained from the general equation (28) by recalling that ρ_g approaches zero as the pore width and adsorbed layer thickness become small. Further, the adsorbed layers on opposing pore walls also merge in this limit, so the surface tension term additionally vanishes. This leaves a simple relationship between the condensation pressure and the pore averaged potential field.

$$\ln\left(\frac{p}{p_0}\right) \approx \frac{V_w}{kT\widehat{w}} = \bar{V}^* \qquad (33)$$

When these two quantities are equal, the energy of the condensed liquid is nearly zero (see Fig. 3) and is therefore approximately equal to the negligibly small energy of the low density gas that occupied the pore prior to condensation. This interpretation applies to continuous phase transitions in pores smaller than two molecular diameters, precisely the regime in which the asymptotic approximation merges with the general equation.

In large pores, or equivalently at high pressures, the NG equation reduces to the well known Kelvin relationship in which surface tension plays a dominant role.

$$\ln\left(\frac{p}{p_0}\right) \approx -\frac{2\Gamma}{kT\rho_0(\widehat{w} - 2\widehat{\delta})} \approx -\frac{2\gamma}{kT\rho_0 w} \qquad (34)$$

The integrals of the wall potential, V_w and V_δ, do not appear here because they become equal and offsetting when the adsorbed layers extend to ranges where the wall potential becomes negligible. The other simplifications arise because $\rho_g \approx \rho_0$ and $\widehat{\delta} << \widehat{w}$.

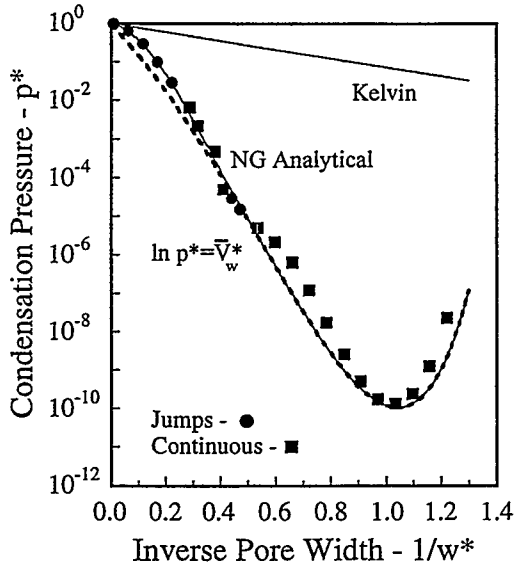

Figure 6. Computed condensation pressures of the present NG equation (solid line) are in good agreement with those obtained by numerical solution of the full DFT equations (symbols). Dotted line is the small-pore asymptote of the NG equation.

Results: Implicit Analytical Model

Since the pressure appears in Eq. (29) describing the adsorbed layer thickness, it is not yet possible to simply select a value of the pore width and explicitly calculate the corresponding pore pressure from Eq. (28). Instead, a root finder or iterative procedure must be used to find the particular value of the pressure for which the two sides of Eq. (28) are equal. This shortcoming will be remedied later by combining a pair of asymptotic expressions that apply to large pores. However, before introducing that approximation, we will first explore the accuracy of the implicit form of the equations given in the preceding section by comparison with numerical DFT results.

An implicit calculation of the pore pressure proceeds as follows. First, select a pore width and evaluate V_w. Then, for a guessed value of the condensation pressure calculate: $\widehat{\delta}$ from (29)-(31), V_δ from (26), Γ from (27), and ρ_g from (32). Substitute all of these results into the condensation equation, (28), check for equality, and repeat to convergence. All of the algebra is simple, and the iterations can be implemented either by using standard root finding routines or by simply substituting a guess into the right side of Eq. (28) and using the resulting left hand side as the next guess.

Figure 6 shows a comparison of the condensation pressures calculated by the implicit analytical model with those computed numerically by DFT. The full NG equation is represented by a solid curve; the dashed curve represents the small-pore asymptote of the model as given by Eq. (33). In the numerical approach, both the liquid and gas-like density and energy profiles are calculated for a large number of pressures to accurately determine the particular pressure at which the two solutions have equal energy. These numerically calculated condensation pressures are indicated by two types of symbols. The circles represent solutions having a density jump at the condensation point, whereas squares denote the point of steepest density increase during continuous phase transitions.

The analytical model is clearly in good agreement with the numerical calculations over the full range of pore sizes. As seen in the upper left of Fig. 6, agreement is best for larger pore widths, or equivalently, for smaller values of the inverse pore width. Indeed, the maximum relative deviation from the condensation pressures computed by numerical DFT is less than 6% for all pore widths greater than four ($1/w^* < 0.25$). This covers much of the range of practical interest.

In smaller pores the accuracy of the NG equation is diminished somewhat by steric effects associated with non-integer values of the normalized pore width. For example, a sharp decrease in the condensation pressure computed by DFT occurs when the pore can no longer accommodate a pair of molecular layers at their preferred spacing, σ. This drop occurs at $\widehat{w}^* \approx 2$, corresponding to $w^* = 2.66$ and $1/w^* = 0.38$. In yet smaller pores, the repulsion between confined molecular layers becomes so great that only a single molecular layer can fit between the pore walls. Condensation in these very small pores occurs by a continuous transition, making it difficult even to define a distinct condensation pressure. These things considered, the analytical condensation formula still provides remarkable agreement with detailed DFT calculations.

The curious rise in the condensation pressure seen in Fig. 6 for very small pores is a consequence of the overlapping energy minima of the Lennard-Jones wall potentials. The minimum condensation pressure of $p^* \approx 10^{-10}$ occurs when the energy minima of both wall potentials are exactly coincident in the pore center. When the spacing is either larger or smaller, the misalignment of the potential wells weakens the effective potential field. A weaker attractive field is unfavorable to the formation of a liquid, so a greater pressure is required to produce condensation.

Analytical and numerical calculations of the normalized adsorbed layer thickness, $\delta^* = \delta/\sigma$, are compared in Fig. 7. Symbols represent DFT results, the

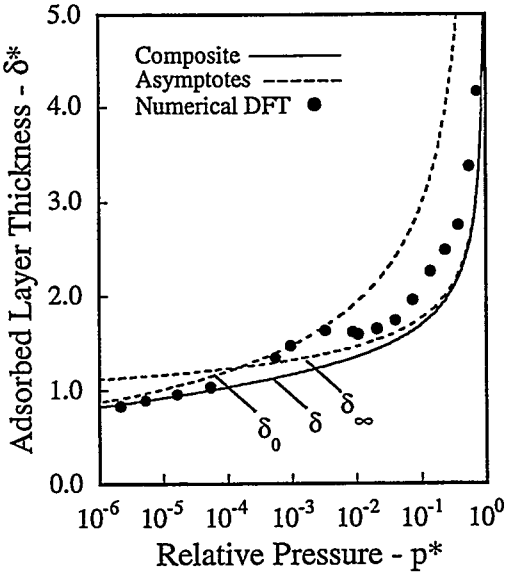

Figure 7. Adsorbed layer thicknesses given by composite analytical formula (solid line) are consistent with numerical DFT results (symbols). Dotted lines indicate asymptotes of composite formula.

solid line is the composite analytical formula given by Eq. (31), and the two dashed lines indicate the asymptotic expressions for small and large pores. The transition between asymptotes occurs at a relative pressure of $p* \approx 10^{-4}$, corresponding to a pore size of $\widehat{w}^* \approx 2$, in keeping with physical interpretations of the small pore limit. Since δ does not appear explicitly in the numerical DFT calculations, it is determined by equating the total mass of adsorbed gas, obtained by integration of the DFT profiles, to twice the product of the adsorbed layer thickness and the mean layer density, ρ_g. For consistency, ρ_g, is evaluated using the analytical expression given earlier.

$$\int_0^w \rho\, dx = 2\rho_g \widehat{\delta} \quad \text{where} \quad \rho_g = \rho_0\Big(\frac{2\widehat{\delta}-1}{2\widehat{\delta}}\Big) \qquad (35)$$

When combined, these two relations yield a simple expression for the value of $\widehat{\delta}$ corresponding to the gas-like DFT solution at the condensation pressure. In very small pores, this value of $\widehat{\delta}$ is limited to be no more than half the reduced pore width, $\widehat{w}$.

These numerically calculated layer thicknesses, shown by symbols in Fig. 7, generally lie above the solid line representing the composite analytical model. The agreement could be noticeably improved by simply adding about $\sigma/2$ to the numerical value of the large-pore asymptote. We hesitate to make this adjustment partly because the asymptote, as it stands, is

in relatively good agreement with experimental measurements of adsorption on flat surfaces. In addition, the moderate disagreement in adsorbed layer thickness, between analytical and numerical models, has not significantly degraded the excellent agreement in calculated condensation pressures.

Results: Explicit Analytical Model

The preceding system of equations is implicit in the sense that the condensation pressure appears on both sides of Eq. (28). This can be remedied by combining our previous expression for the adsorbed layer thickness in large pores, Eq. (29), with the Kelvin expression for the condensation pressure in large pores, Eq. (34). Eliminating the pressure between these two equations yields the following relationship between the pore width and the adsorbed layer thickness just prior to condensation.

$$\widehat{\delta}_{\infty}^{3} = \frac{A\,kT\,\rho_0\,w}{2\gamma} = \frac{\rho_0\,w\epsilon_w\sigma_{sf}^4}{6\gamma\Delta} \qquad (36)$$

The constant, A, appearing here was defined previously in Eq. (29). As before, this asymptotic expression for large pores is blended with the small pore asymptote by introducing both into Eq. (31).

An explicit calculation of the condensation pressure requires no iteration. For a chosen pore width, $\widehat{\delta}$ is first determined from the preceding equation together with Eqs. (30) and (31). V_δ, V_w, Γ, and ρ_g then follow from Eqs. (26), (27), and (32). Substitution of these results into Eq. (28) yields the condensation pressure. The entire procedure is easily performed, even in a spread-sheet environment.

The condensation pressures computed in this explicit manner are nearly indistinguishable from those obtained earlier using the implicit formulation. Thus, there is no need to present another plot like Fig. 6. The maximum deviation of the explicit model from the numerically calculated condensation pressures is about 10% for $w^* \geq 5$, as compared with about 6% for the implicit formulation. This close agreement between the implicit and explicit models is not surprising, since both versions must approach the same asymptotes for both small and large pores.

Differences between the implicit and explicit analytical models are most apparent in comparing calculated values of the adsorbed layer thickness. As shown in Fig. 8, the explicit model yields somewhat larger values of the absorbed layer thickness, in better agreement with the numerical DFT calculations. Also, since the mean adsorbed layer density, ρ_g, increases with δ, the explicitly calculated density is

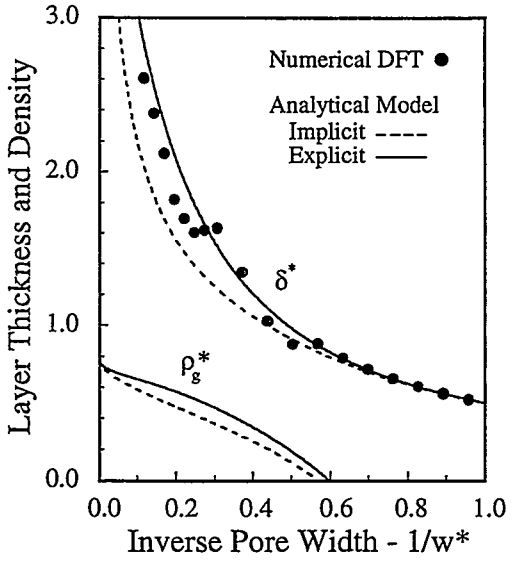

Figure 8. Numerical calculations of adsorbed layer thickness (symbols) are bounded by implicit and explicit forms of the present analytical model. Mean layer density prior to condensation is also shown.

greater than that calculated implicitly. Values of the layer density computed by DFT are not included in Fig. 8 because of the ambiguity involved in separately determining ρ_g and δ when only their product is constrained by the numerical solutions.

Comparison with Modified Kelvin Equation

Figure 9 shows a comparison between the present explicit analytical model and two well known analytical approximations. The first of these is the Kelvin equation [1,2]. Although exact for very large pores, this relation becomes a very poor approximation for the smaller pores of greatest practical interest in applications of microporous materials. The modified Kelvin (MK) equation, also shown in Fig. 9, extends the range of validity to smaller pore sizes by using an apparent pore width obtained by reducing the nominal width by the combined thickness of the two adsorbed layers [4,9]. The physical motivation for this is obvious and the resulting equation is simple.

$$\ln\left(\frac{p}{p_0}\right) = -\frac{2\gamma}{kT\rho_0(w-2\delta)} \qquad (37)$$

The value of δ used in the effective pore width, $w-2\delta$, is usually obtained either from experimental data or from analytical approximations like Eq. (29) describing adsorption on an external surface. Since either of

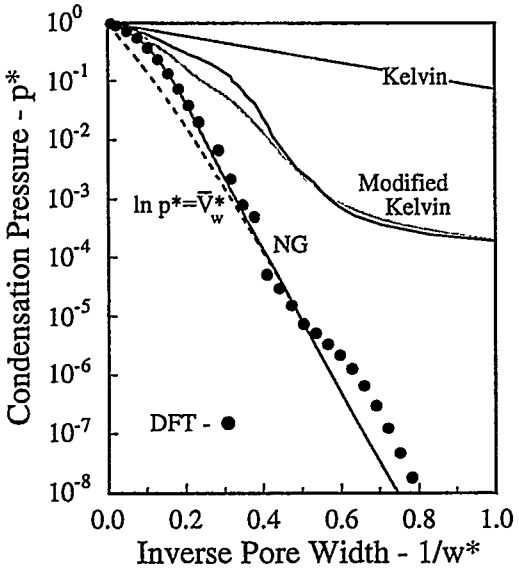

Figure 9. Traditional Modified Kelvin (MK) equation severely over-predicts condensation pressures for small pores. Upper and lower MK curves are respectively based on experimental and DFT values of $\delta(p)$.

these approaches provides δ as a function of pressure, the MK equation becomes implicit in the pressure and must generally be solved iteratively. However, the MK equation can be inverted to the following form

$$w = 2\delta - \frac{2\gamma}{kT\rho_0 \ln(p/p_0))} \tag{38}$$

which permits direct calculation of the pore width corresponding to a particular condensation pressure and corresponding value of $\delta(p)$.

The MK equation usually yields condensation pressures somewhere between those of the Kelvin equation and the correct values, as apparent in Fig. 9. Two different evaluations of the MK equation are included in Fig. 9. The upper curve is based on a number of consistent data sets for adsorption of nitrogen on a flat graphite surface [2,15,16]. The lower of the two MK curves was constructed using values of $\delta(p)$ computed numerically by DFT. We see that the MK equation is in error by a factor of two when the condensation pressure has been reduced by a factor of five or ten, and that the error in pressure reaches one or two orders of magnitude for pores smaller than three or four molecular diameters. In contrast, the NG equation remains accurate within a few percent throughout this range.

The failure of the MK equation results from two fundamental shortcomings. First and foremost, the MK equation does not directly account for the effect of the wall potential, $\bar{V}^*$ on the liquid energy. Yet, this is the dominant physical considerations in small pores where the condensation pressure is well approximated by $\ln p^* = \bar{V}^*$. Thus, any MK equation that excludes this effect is certain to fail in the small pore limit.

The second shortcoming of the conventional MK equation is that the adsorbed layer thickness, $\delta(p)$, is generally based on measured or calculated values of the amount of gas adsorbed on a flat external surface. In small pores, however, the adsorbed layers form at much lower pressures because of the superposed fields of both pore walls. Thus, the effective pore width, $w - 2\delta$, appearing in the denominator of the MK equation is too large, resulting in a condensation pressure which is far too great (i.e., magnitude of logarithm too small). If instead, we use a better estimate of the adsorbed layer thickness, like the present composite Eq. (31), the denominator of the MK equation will approach zero as δ approaches $w/2$, resulting in a condensation pressure that is far too small. Thus, the MK equation is not readily salvaged by a better choice of δ. Instead, as apparent in deriving the NG equation, the denominator should contain the group $\rho_\ell w - 2\rho_g\delta$, which approaches $\rho_\ell w$ rather than $\rho_\ell(w - 2\delta)$ as $\rho_g \to 0$.

Required Material Property Information

Use of the NG equation requires only a minimal description of the interaction of fluid molecules with one another and with the adsorbent surface. The fluid-fluid interaction is most easily given in terms of the nominal liquid density, $\rho_\ell = \rho_0$, the Lennard-Jones diameter, σ, and the surface tension, here taken at the textbook value of $\gamma = 8.88$ mN/m for nitrogen at 77 K [2]. The parameter ϵ_{ff} does not appear explicitly in the final equations, though it is implicit in the surface tension. The fluid-solid interaction is described here in terms of the Lennard-Jones parameters ϵ_{sf}, σ_{sf}, ρ_s and Δ appearing in the constant, ϵ_w, that scales the wall potential function, V. The values of these parameters for nitrogen adsorption on graphite were given above Eq. (14) and are available for many common gas and solid pairs.

The material parameters listed above include a mixture of macroscopic and microscopic properties that are chosen mainly for ease of use. For example, we have chosen to use the surface tension and nominal liquid density to characterize the fluid, since these macroscopic properties are widely available and appear explicitly in our analytical model. However, the density and surface energy can alternatively be calculated from the Lennard-Jones parameters of the

fluid using the equations of DFT, either approximately based on the simplified bulk fluid equations or more exactly by performing a numerical calculation. In this context, it should be noted that the value of the Lennard-Jones energy, ϵ_{ff}, used in our simulations was chosen so that the bulk energy of the gas and the liquid phases, given by Eq. (17), would be identical at 101 kPa and 77 K, in keeping with measured conditions of phase equilibrium.

As a consistency check, DFT was used to compute the surface energy associated with a one dimensional density profile that transitions smoothly between liquid and vapor densities. The calculated surface energy at the reference state (saturation pressure at 77 K) was within a few percent of the accepted value of γ noted just above. Thus, a single value of the Lennard-Jones energy, ϵ_{ff}, yields correct and self-consistent DFT results for both the bulk condensation pressure and the surface tension as well as the liquid density.

The fluid-solid interaction is described here in terms of the Lennard-Jones parameters σ_s, Δ_s, and ϵ_w appearing in the integrated wall potentials, V_w and V_δ, and in the asymptotic formula for the adsorbed layer thickness, $\delta(p)$. Although the effective molecular diameters are usually known within reasonable limits, the interaction energy, ϵ_w, is not always available. However, this parameter can be deduced from the adsorption isotherm measured on a flat surface. The initial slope of the isotherm, known as Henry's constant, is related to ϵ_w through the following form of Eq. (14)

$$\frac{d\rho}{dp} = \frac{1}{kT} e^{-\epsilon_w V'/kT} \tag{39}$$

which is applicable at low pressures where fluid-fluid interactions are unimportant. Here, $V' = V/\epsilon_w \approx -0.68$ is the value of the wall potential function in the first adsorbed layer. The numerical value of -0.68 corresponds to the minimum of V occurring at the center of the first molecular layer. It is, however, preferable to use the exponentially weighted average of V over the first molecular layer, roughly -0.58 for Steele's graphite potential. Either way, ϵ_w can be estimated from the initial slope of the adsorption isotherm.

The measured adsorption isotherm of a flat surface also provides a description of the adsorbed layer thickness as a function of pressure, $\delta_\infty(p)$, applicable to wide pores. This data can be used in its primitive tabular form or, alternatively, approximated by an analytical function like Eq. (29). This data or function is then combined with Eqs. (30) and (31) to construct a composite function representing $\delta(w)$ at condensation. Further, for adsorbed layers thicker than two or three molecular diameters we earlier observed that

$$V^*(x^*) \approx \ln p^* \qquad \text{at} \qquad x^* = \delta^*(p^*) \tag{40}$$

Thus, for a given pressure, the value of V^* can be calculated and the corresponding values of δ can be read from a measured adsorption isotherm. This process may be used to construct the asymptotic form of the wall potential, $V^*(x^*)$.

Finally, it is important to recognize that the interaction energy, ϵ_w affects both the initial slope (Henry's constant) and the asymptotic behavior of a measured adsorption isotherm. Thus, experimental observations of both quantities may be used to verify or improve the functional form of the wall potential. Once this function has been decided upon, in either analytical or tabular form, it may be introduced into the equations relating the condensation pressure to the pore width. In deriving these equations we have made no assumptions regarding the form of the wall potential.

Summary

The governing equations of Density Functional Theory (DFT) have been used to derive an analytical expression for the fluid condensation pressure in slit pores bounded by parallel plane walls. First, by integrating the DFT equations over a bulk fluid it was shown that the fluid energy, averaged over molecular scales, can be well approximated by a simple expression that depends only on the ambient temperature and pressure and the external potential field. The total energy within a slit pore was then written as an integral of the local energy over the pore width, assuming uniform density within regions occupied by liquid or adsorbed layers.

Prior to condensation, virtually all of the fluid energy resides within the adsorbed layers on the pore walls; the energy of the gas in the pore center is negligible. After condensation, the pore is filled with liquid. To define the condensation pressure, we equated integral expressions describing the total pore energy before and after condensation. At lower pressures, the adsorbed layers have less energy than a liquid-full pore, while at higher pressures the reverse is true. So, the transition is defined by equality of energy.

The resulting analytical expression relates the condensation pressure to all of the important physical parameters governing adsorption and condensation over the full range of pore sizes. Its most general form is given by

$$\ln\left(\frac{p}{p_0}\right) = \frac{\rho_\ell V_w - \rho_g V_\delta - 2\Gamma}{kT(\rho_\ell \widehat{w} - 2\rho_g \widehat{\delta})}$$

in which the eight parameters and functions on the right-hand side are: the temperature, T, pore width, $\widehat{w}$, nominal liquid density, ρ_ℓ, surface tension, Γ, two integrals of the wall potential, V_w and V_δ, and the thickness, $\widehat{\delta}$, and density, ρ_g, of the adsorbed layers prior to condensation. These last two quantities are replaced by composite functions of pressure and pore width constructed from asymptotic expressions applicable in the limits of small and large pores.

Use of this simple expression requires only a knowledge of the nominal liquid density, surface tension, and molecular diameter of the fluid as well as the Lennard-Jones parameters (energy and range) of the interaction between fluid molecules and the pore walls. If unavailable, the interaction energy can be deduced from the measured adsorption isotherm for a flat surface. Although our illustrative calculations are for a Lennard-Jones wall potential, any alternative potential may also be used in conjunction with the fundamental condensation equation.

In the large pore limit, the condensation equation derived here is equivalent to the Kelvin equation in which surface tension plays a dominant role. In the small pore limit, our equation reduces to an equally simple relationship between the condensation pressure and the pore averaged potential field. The transition between these regimes is controlled by the transitional behavior of the composite functions describing the density and thickness of the adsorbed layers.

Two different forms of our condensation equation were presented. The implicit form contains the pressure on both sides of the equation and must be solved by iteration. The alternative explicit form was obtained by using a pair of asymptotic expressions to eliminate the pressure from the large-pore asymptote of the adsorbed layer thickness. Both the implicit and explicit equations agree with detailed DFT calculations within a few percent for pores in which the phase transition occurs abruptly at a distinct pressure. For very small pores, the predicted condensation pressure coincides with the steepest portion of the continuous transition between gas and liquid densities.

The present analytical model differs from previous pore condensation equations in two primary respects. First, a single equation provides very accurate values of the condensation pressure over the full range of pore sizes. Second, this equation is derived from a general theory (DFT) that provides a fundamental basis for understanding, testing, and improving the approximations fundamental to its development.

Nomenclature

d	molecular diameter used to calculate repulsions
f	Helmholtz free energy per unit volume
k	Boltzmann's constant
p	pressure
$\mathbf{r}$	position vector
T	temperature
u	Lennard-Jones pair potential
U	fluid-fluid attraction
V	external potential induced by solid walls
V_w	integral of V over reduced pore width
V_δ	integral of V over reduced film thickness
w	pore width
$\widehat{w}$	reduced pore width, $w - 2\epsilon$
x	distance from solid surface
z	distance from center plane of wall molecules
δ	thickness of adsorbed film
$\widehat{\delta}$	reduced film thickness, $\delta - \epsilon$
δ_0	asymptotic film thickness in small pores
δ_∞	asymptotic film thickness in large pores
Δ	basal plane spacing of wall molecules
$\Delta\psi$	excess hard sphere repulsion
ϵ	width of excluded zone near pore wall ($\approx\sigma/3$)
ϵ_{ff}	energy well depth of fluid-fluid potential
ϵ_{sf}	energy well depth of fluid-solid potential
ϵ_w	pre-multiplier of Steele's graphite potential
η	volume fraction occupied by molecules
Λ	de Broglie wavelength
μ	chemical potential
ρ	fluid density in molecular masses per unit volume
$\widehat{\rho}$	locally averaged density used in repulsion
σ	molecular diameter
Ω	grand potential energy functional

Subscripts

g	gas
ℓ	liquid
0	condensation point of bulk fluid

Superscripts

$'$	derivative or integration variable
$*$	normalized quantity (length scaled by σ)
$-$	averaged over pore width or layer thickness

Acknowledgment

This work was sponsored by the Engineered Materials and Processes Research Foundation at Sandia National Laboratories. Sandia is a multiprogram laboratory operated by Sandia Corporation, a Lockheed Martin Company, for the United States Department of Energy under contract DE-AC04-94AL85000.

Appendix: Integrals of the External Potential

The integrals, V_w and V_δ, defined by Eq. (26) can be evaluated by analytically integrating the Steele potential of Eqs. (8)-(10). The result may be stated as follows

$$V_\delta = I(\delta) \quad \text{and} \quad V_w = I(w/2) \tag{A1}$$

where each I includes contributions from both near and far pore walls, shown below on separate lines.

$$I(x) = 2\,\epsilon_w \sigma_{sf} \left[\widehat{v}\,(x + \frac{\sigma_{sf}}{2}) - \widehat{v}\,(\epsilon + \frac{\sigma_{sf}}{2}) + \widehat{v}\,(w - \epsilon + \frac{\sigma_{sf}}{2}) - \widehat{v}\,(w - x + \frac{\sigma_{sf}}{2}) \right] \tag{A2}$$

The function $\widehat{v}\,(z)$ is simply the integral of $v(z)$ given in Eq. (8).

$$\widehat{v}\,(z) = -\left[\frac{2}{45} \left(\frac{\sigma_{sf}}{z} \right)^9 - \frac{1}{3} \left(\frac{\sigma_{sf}}{z} \right)^3 - \frac{\sigma_{sf}^3}{6\Delta(z+0.61\Delta)^2} \right] \tag{A3}$$

In the last two equations, x is measured from the pore wall while z is measured from the center of the outermost wall molecules. Hence, $z = x + \sigma_{sf}/2$ for the near pore wall, and $z = w - x + \sigma_{sf}/2$ for the far pore wall, as apparent in Fig. 2.

References

1. D. M. Ruthven, *Principles of Adsorption and Adsorption Processes*, Wiley-Interscience, NY, 1984.

2. S. J. Gregg and K. S. W. Sing, *Adsorption, Surface Area, and Porosity*, Academic Press, London, 1983.

3. M. M. Dubinin, "Fundamentals of the Theory of Adsorption in Micropores of Carbon Adsorbents: Characteristics of Adsorption Properties and Microporous Structures", *Carbon*, Vol. 27, No. 3, 457-467, 1989.

4. N. A. Seaton, J. P. R. B. Walton, and N. Quirke, "A New Analysis Method for the Determination of the Pore Size Distribution of Porous Carbons from Nitrogen Adsorption Measurements", *Carbon*, Vol. 27, No. 6, 853-861, 1989.

5. C. Lastoskie, K. E. Gubbins, and N. Quirke, "Pore Size Distribution Analysis of Microporous Carbons: A Density Functional Theory Approach", *J. Phys. Chem.*, Vol. 97, No. 18, 4786-4796, 1993.

6. J. P. Olivier, W. B. Conklin, and M. V. Szombathely, "Determination of Pore Size Distributions from Density Functional Theory: A Comparison of Nitrogen and Argon Results", *Characterization of Porous Solids III*, edited by J. Rouquerol, F. Rodriguez-Reinoso, K. S. W. Sing, and K. K. Unger, Studies in Surface Science and Catalysis, Vol. 87, 81-89, Elsevier Science, 1994.

7. R. H. Nilson and S. K. Griffiths, "A Locally Analytic Density Functional Theory Describing Adsorption and Condensation in Microporous Materials", *J. Chem. Phys.*, Vol. 108, No. 3, 1162-1174, 1998.

8. S. Brunauer, L. E. Copeland, and D. L. Kantro, *The Langmuir and BET Theories*, The Solid-Gas Interface, edited by E. A. Flood, Marcel Dekker NY, 1967.

9. W. A. Steele, *The Interaction of Gases with Solid Surfaces*, Pergamon Press, Glasgow, 1974.

10. G. Horvath and K. Kawazoe, "Method for the Calibration of Effective Pore Size Distribution in Molecular Sieve Carbon", *J. Chem. Eng. Japan*, Vol. 16, No. 6, 470-475, 1983.

11. A. Saito and H. C. Foley, "Curvature and Parametric Sensitivity in Models for Adsorption in Micropores", *AIChE Journal*, Vol. 37, No. 3, 429-435, 1991.

12. D. E. Sullivan and M. M. Telo de Gama, *Wetting Transitions and Multilayer Adsorption at Fluid Interfaces*, Fluid Interfacial Phenomena, edited by C. A. Croxton, John Wiley, NY, 1986.

13. P. Tarazona, "Free-energy Functional for Hard Spheres", *Phys. Rev. A*, Vol. 31, No. 4, 2672-2679, 1985.

14. A. Papadopoulou, F. van Swol, U. Marini, and B. Marconi, "Pore-end Effects on Adsorption Hysteresis in Cylindrical and Slitlike Pores", *J. Chem. Phys.*, Vol. 97, No. 9, 6942-6952, 1992.

15. C. Lastoskie, K. E. Gubbins, and N. Quirke, "Pore Size Heterogeneity and the Carbon Slit Pore: A Density Functional Theory Model", *Langmuir*, Vol. 9, 2693-2702, 1993.

16. J. P. Olivier and W. B. Conklin, "Determination of Pore Size Distributions from Density Functional Theoretic Models of Adsorption and Condensation within Porous Solids", in DFT Software, available from Micromeritics Instrument Corporation, Norcross, GA, 30093, 1993.

UNLIMITED RELEASE
INITIAL DISTRIBUTION

K. F. Jensen
Massachusetts Institute of Technology
Building 6-469
Chemical Engineering
Cambridge, MA 02139

B. W. Sheldon
Division of Engineering, Box D
182 Hope Street
Providence, RI 02912

G. S. Thurston
Integrated Systems, Inc.
300 W. Main Street
Northborough, MA 01532

R. J. Kee
Engineering Division
Colorado School of Mines
Golden, CO 80401-1887

0513 R. J. Eagan, 1000
1435 K. A. Hays, 1800
1434 G. E. Pike, 1802
0367 P. A. Cahill, 1812
1413 T. A. Michalske, 1114
1407 C. L. Renschler, 1812
1407 J. H. Aubert, 1815
1407 R. R. Lagasse, 1815
1349 C. J. Brinker, 1815
0710 G. A. Carlson, 6211
9001 T. O. Hunter, 8000
Attn: M. E. John, 8100
R. C. Wayne, 8400
D. L. Crawford, 8900
9671 J. S. Schoniger, 8120
9214 C. F. Melius, 8130
9420 L. A. West, 8200
9405 J. M. Hruby, 8230
9405 L. L. Whinnery, 8230
9054 W. J. McLean, 8300
Attn: L. A. Rahn, 8351
F. P. Tully, 8353
D. R. Hardesty, 8361
R. W. Carling, 8362
9163 W. Bauer, 8302
9042 G. H. Evans, 8345
9042 J. F. Grcar, 8345
9042 S. K. Griffiths, 8345 (10)
9041 J. S. Binkley, 8345
9042 R. S. Larson, 8345
9042 R. H. Nilson, 8345 (10)
9051 P. H. Paul, 8351
9671 D. W. Arnold, 8358
9405 T. M. Dyer, 8700
Attn: C. M. Hartwig, 8701
M. I. Baskes, 8712
G. J. Thomas, 8715
K. L. Wilson, 8716
S. M. Foiles, 8717
9403 W. R. Even, 8713
9403 T. J. Shepodd, 8713
9403 J. C. F. Wang, 8713
0841 P. J. Hommert, 9100
0834 A. C. Ratzel, 9112
0834 M. J. Martinez, 9112
0834 W. L. Hermina, 9111
0826 M. R. Baer, 9112
0827 C. C. Wong, 9114
1111 L. J. Frink, 9225
1111 F. B. Van Swol, 9225

9018 Central Technical Files, 8940-2 (3)
0899 Technical Library, 4916 (1)
9021 Technical Communications, 8815
Technical Library, MS 0899, 4916 (1)
9021 Technical Communications, 8815
For DOE/OSTI (1)